Clim. Past Discuss., https://doi.org/10.5194/cp-2019-4
Manuscript under review for journal Clim. Past
Discussion started: 21 January 2019

Climate of the Past Discussions

The drivers of late Quaternary climate variability in eastern South Africa

Charlotte Miller[1*], Jemma Finch[2], Trevor Hill[2], Francien Peterse[3], Marc Humphries[4], Matthias Zabel[1], Enno Schefuß[1]

[1]MARUM - Center for Marine Environmental Sciences, University of Bremen, Bremen, Germany
[2]School of Agricultural, Earth and Environmental Sciences, University of KwaZulu-Natal, Pietermaritzburg, South Africa
[3]Department of Earth Sciences, Utrecht University, Netherlands
[4]Molecular Sciences Institute, School of Chemistry, University of the Witwatersrand, Johannesburg, South Africa

*Correspondence email: lottiemiller2@gmail.com

Abstract

The scarcity of continuous, terrestrial, palaeoenvironmental records in eastern South Africa leaves the evolution of late Quaternary climate and its driving mechanisms uncertain. Here we use a ~7-m long core from Mfabeni peatland (KwaZulu-Natal, South Africa) to reconstruct climate variability for the last 32 thousand years (ka BP). We infer past vegetation and hydrological variability using stable carbon ($\delta^{13}C_{wax}$) and hydrogen isotopes (δD_{wax}) of plant-wax *n*-alkanes and use P_{aq} to reconstruct water table changes. Our results indicate that late Quaternary climate in eastern South Africa did not respond directly to orbital forcing nor to changes in sea surface temperatures (SSTs) in the western Indian Ocean. The arid conditions evidenced at Mfabeni during the Last Glacial Maximum (LGM) are a consequence of both low SSTs and an equatorward displacement of the southern hemisphere westerlies due to increased Antarctic sea ice extent. The increased humidity at Mfabeni between 19–14 ka BP likely resulted from decreased Antarctic sea ice which led to a southward retreat of the westerlies and increased the influence of the moisture-bearing tropical easterlies. Between 14–5 ka BP, when the westerlies were in their southernmost position, local insolation became the dominant control, leading to stronger atmospheric convection and an enhanced tropical easterly monsoon. Generally drier conditions persisted during the past *c.* 5 kyrs, but were overlain by high amplitude, millennial-scale environmental variability, probably resulting from an equatorward return of the southern hemisphere westerlies and heightened ENSO activity. Our findings stress the influence of the southern hemisphere westerlies in driving climatological and environmental changes in eastern South Africa.

Key words: Mfabeni; eastern South Africa; *n*-alkanes; hydrogen isotopes; carbon isotopes; southern hemisphere westerlies; tropical easterlies

1. Introduction

Last glacial (*c.* 21 ka BP) to present-day changes in vegetation, precipitation and temperature in eastern South Africa are poorly constrained. Whether eastern South Africa was characterized by aridity or increased humidity during the last glacial period remains unclear. Proxy data show spatial complexity (e.g. Baker et al., 2016; Chase et al., 2017; Chevalier and Chase, 2015 & 2016, Dupont et al., 2011; Schefuß et al., 2011; Scott et al., 2012; Scott, 2016; Schmidt et al., 2014; Simon et al., 2015), and modelled LGM precipitation for the region are highly variable and often do not even agree on the sign of precipitation change. For example, the PMIP3 model ensemble mean suggests increased last glacial precipitation in the east of South Africa with dry conditions towards the north and south (compared to the present day; Braconnot et al., 2007). Conversely, the NCAR CCSM3 model indicates drier than present conditions in the centre of South Africa and along the eastern coast (Otto-Bliesner et al., 2006). These contrasting simulations for the last glacial period highlight the difficulty in simulating past precipitation in South Africa with a lack of proper understanding of relevant processes (Stone, 2014).

The mechanisms driving Quaternary climate variability in South Africa are complex and spatially heterogeneous. For example, hydroclimate may be paced by austral summer insolation fluctuations, resulting from changes in the Earth's orbital precession on 23–19 ka timescales. Strong summer insolation (during precession maxima) causes stronger atmospheric convection and an increase in the land/ocean temperature contrast, which results in higher moisture transport by the tropical easterlies and higher precipitation in eastern South Africa (e.g. Simon et al., 2015). Climate may also be influenced by high-latitude forcing related to changes in the Earth's orbital obliquity and eccentricity on longer, i.e. glacial-interglacial timescales, which may result in latitudinal contraction and expansion of the climatic belts (e.g. Dupont, 2011). The model of Nicholson and Flohn (1980) suggests an equatorward displacement of the intertropical convergence zone (ITCZ; Fig. 1) during the last glacial period, although proxy data from South Africa provide no conclusive support for this scenario. In addition, during glacial periods, the Walker Circulation may have been weaker with its ascending limb further to the east, within the Indian Ocean. This possibly resulted in an eastward displacement of the coastal cloud band and thus a drier summer rainfall zone (SRZ) and a wetter winter rainfall zone (WRZ; Tyson, 1986). Furthermore, changes in the latitudinal position of the southern hemisphere westerlies (as a response to fluctuations in Antarctic sea ice extent) have been invoked to influence climate in South Africa (Chase and Meadows, 2007; Chevalier and Chase, 2015; Chase et al., 2017). The western South African region has received most focus regarding the southern hemisphere westerly influence

Clim. Past Discuss., https://doi.org/10.5194/cp-2019-4
Manuscript under review for journal Clim. Past
Discussion started: 21 January 2019

Climate of the Past Discussions Open Access EGU

in controlling climate variability (e.g. Zhao et al., 2016; Burdanowitz et al., 2018). Some studies suggest possible mechanistic links between SSTs in the Agulhas Current and the Indian Ocean and rainfall variability in South Africa, with high SSTs linked to increasing South African summer precipitation (e.g. Baker et al., 2017; Chase et al., 2017; Dupont, 2011; Dupont et al., 2011; Reason and Mulenga, 1999).

The spatially heterogeneous nature of climate variability in South Africa from the last Glacial to the present-day, and the multiple possible climate drivers render the region an important focus for palaeoclimate research. Two important questions remain: i) what was the climate like in eastern South Africa during the last Glacial period? and, ii) what were the causes for the climate variability? These questions are difficult to answer with the majority of long, continuous, terrestrial records situated within the range of the modern ITCZ (Fig. 1; *c*. 14°S, e.g. Barker et al., 2007; Tierney et al., 2008), making it hard to assess the long-term climate drivers further south, in particular in eastern South Africa. In this area, terrestrial sediment archives suitable for palaeoenvironmental reconstruction are scarce, in particular those extending into the LGM. Marine and speleothem archives have hitherto mostly formed the basis of Quaternary climate research in this region (e.g. Chevalier and Chase, 2015; Dupont et al., 2011; Holmgren et al., 1999). Here we provide stable carbon ($\delta^{13}C$) and hydrogen (δD) isotope records of terrestrial plant-waxes (long-chained *n*-alkanes) from Mfabeni peatland. Our vegetation and hydroclimate reconstructions are compared with a previous biomarker-palaeoclimate study from Mfabeni (Baker et al., 2014, 2016 & 2017). We more than double the temporal resolution of the previous plant-wax $\delta^{13}C$ record from Baker et al. (2017), from *c*. 1200 to *c*. 500 years, revealing important and previously undocumented environmental variability.

2. Regional setting

South Africa is divided into three main rainfall zones, i) the summer rainfall zone (SRZ), ii) the winter rainfall zone (WRZ), and iii) the overlapping year-round rainfall zone (YRZ; Fig. 1; Chase and Meadows, 2007). The SRZ lies in the north and east where 66 % of the mean annual precipitation falls between October and March (Chase and Meadows, 2007). Within the SRZ the climate is dominated by tropical temperate troughs and easterly flow, which brings moisture from the Indian Ocean to eastern South Africa. In the south and west of South Africa lies the WRZ, where 66 % of the mean annual precipitation falls between April and September (Chase and Meadows, 2007). This rainfall is associated with temporal frontal systems related to the southern hemisphere westerlies (Mason and Jury, 1997). Sandwiched between the SRZ and WRZ lies the YRZ, which receives precipitation both in summer and winter seasons. This zone comprises much of the southern Cape of South Africa and is highly heterogeneous in terms of precipitation seasonality and amount, spanning some of the wettest (e.g. along the south coast), and driest (e.g. Namib Desert; Williamson, 1997) regions in South Africa.

Clim. Past Discuss., https://doi.org/10.5194/cp-2019-4
Manuscript under review for journal Clim. Past
Discussion started: 21 January 2019

Mfabeni peatland is located within the SRZ, on the coastal plain in northern KwaZulu-Natal (28°09'8.1"S; 32°31'9.4"E; 9 m above sea level; Fig. 1; Fig. 2). It is one of the oldest, continuously growing peatlands in South Africa (Grundling et al., 2013). It lies within a topographical inter-dunal depression between the Indian Ocean to the east and Lake St. Lucia to the west (Fig. 2; Grundling et al., 2013). Towards the ocean, it is bordered by an 80–100 m high vegetated dune barrier, and to the west by the 15–70 m high Embomveni sand dune ridge (Fig. 2). Over the last 44 ka BP, the mire accumulated *c*. 11 m of peat, deposited on top of a basal clay layer (Grundling et al., 2015). This clay layer was crucial in the formation and development of the mire, limiting water loss during low sea level stands (Grundling et al., 2013). Mfabeni is bound to the north and south by beach ridges isolating it from Lake Bhangazi and Lake St. Lucia (Fig. 2; Grundling et al., 2013). When lake levels in Lake Bhangazi are high, minor water exchange between Mfabeni and Bhangazi occurs, but there are no fluvial inputs to either system. Surface drainage occurs southwards towards Lake St Lucia (Fig 1; Fig. 2). The modern climate at Mfabeni is subtropical, with hot and humid summers and relatively mild and dry winters. Mean summer temperatures (November to March) surpass 21 °C and the majority of the annual precipitation occurs during the summer months. The main source of water to Mfabeni is precipitation, predominantly provided in the summer by the tropical easterlies (Fig. 1; Tyson, 1999). Occasional rainfall during the winter months is associated with the passage of cold fronts and strong winds from the south (Kruger et al., 2010). The average annual rainfall amount between 2010 and 2018 at Mfabeni in the winter months (June–August) was measured at 134 mm compared to 426 mm during the summer months (December–February), meaning the majority of rainfall (76 %) falls during the summer months (data from World Weather). A northeast–southwest precipitation gradient is present, with 1200 mm year^{-1} of precipitation in the east decreasing to 900 mm year^{-1} westwards towards Lake St. Lucia (Fig. 1; Fig. 2; Taylor et al., 2006). The wind regime is characterised by moderate northeasterly winds during the summer and more intense southwesterly winds during winter.

The peatland receives groundwater via the swamp forest and the western dunes. This groundwater, which is important in keeping the mire wet during the dry season, discharges towards the center of the peatland and then flows within a sub-surface layer towards the east (Grundling et al., 2015). In the northern and eastern part of the peatland, the vegetation is sedge and reed fen (comprising of sedges and grasses). In the western and southern parts of Mfabeni is swamp forest (Venter, 2003). The modern water balance at Mfabeni is dominated by the interplay between evapotranspiration (ET; 1035 mm) and precipitation (1053 mm). Groundwater inflow (14 mm) and stream outflow (9 mm) have a minor contribution to the modern water balance (all measured between May 2008 and April 2009; Grundling et al., 2015). Changes in regional climate have the potential to influence the fine balance between ET and precipitation. For example, ET is suppressed when cloud cover is increased during the summer months and increased during times of higher wind speed

(Grundling et al., 2015). Furthermore, ET is higher in the swamp forest than in the sedge and reed fen, therefore a change in vegetation composition at Mfabeni has the potential to impact ET rates. The depositional setting of the Mfabeni peatland provides a unique opportunity to reconstruct past eastern South African climate variability at centennial-scale resolution from the Late Pleistocene to the present day.

3. Methodological background

To reconstruct past vegetation and hydroclimate changes we use the distribution, and the carbon and hydrogen isotopic composition, of long chain *n*-alkanes derived from plant-waxes.

3.1 Distributions of plant-waxes

To obtain information on water table variations, we quantify the relative contribution of plant-waxes derived from submerged and floating macrophytes relative to that of emergent and terrestrial plants (P_{aq}). Odd-numbered *n*-alkanes (C_{25}–C_{35}) are derived from the epicuticular wax coating of terrestrial higher plants (Eglinton and Hamilton, 1967). Conversely, aquatic plant-waxes (of submerged macrophyte origin) are dominated by mid-chain *n*-alkanes (typically C_{23} and C_{25}; e.g. Baker et al., 2016; Ficken et al., 2002). Thus we quantify P_{aq} using Equation 1 (Ficken et al., 2000).

$$P_{aq} = (C_{23} + C_{25})/(C_{23} + C_{25} + C_{29} + C_{31}) \qquad \text{Eq. 1}$$

with C_x the amount of each homologue.

To assess *n*-alkane degradation we used the carbon preference index (CPI; Bray and Evans, 1961). The CPI reflects the molecular distribution of odd-to-even *n*-alkanes, within a certain carbon number range (here, *n*-C_{26} to *n*-C_{34}; Equation 2). High CPI values indicate a higher contribution of odd-numbered *n*-alkanes (relative to even), indicating the *n*-alkanes are derived from higher terrestrial plants. Low CPI values indicate either low contribution from terrestrial higher plants or high organic matter degradation (Eglinton and Hamilton, 1967).

$$CPI_{27\text{-}33} = 0.5 * (\Sigma C_{odd27\text{-}33}/\Sigma C_{even26\text{-}32} + \Sigma C_{odd27\text{-}33}/\Sigma C_{even28\text{-}34}) \qquad \text{Eq. 2}$$

with C_x the amount of each homologue.

3.2 Carbon and hydrogen isotopes of terrestrial plant-waxes

To reconstruct vegetation changes, we use the carbon isotopic composition of terrestrial plant-waxes ($\delta^{13}C_{wax}$). On late Quaternary timescales the primary factor determining the amplitude of

Clim. Past Discuss., https://doi.org/10.5194/cp-2019-4
Manuscript under review for journal Clim. Past
Discussion started: 21 January 2019

fractionation between $\delta^{13}C$ of atmospheric CO_2 ($\delta^{13}C_{atm}$) and the carbon isotopic composition of the plant ($\delta^{13}C_{plant}$) is the plant carbon fixation pathway (C_3/C_4/CAM; e.g. Diefendorf and Freimuth, 2017). On these timescales, changes in the $\delta^{13}C_{atm}$ are too small to significantly influence $\delta^{13}C_{wax}$ (Tipple et al., 2010). Shrubs and trees use the C_3 photosynthetic pathway and show the largest fractionation. Grasses utilize either the C_3 or the C_4 pathway, with C_4 plants having the smallest net fractionation (Collister et al., 1994). The differences in carbon isotope fractionation during carbon uptake leads to different $\delta^{13}C_{wax}$ isotopic signatures, and allows the determination of past vegetation types: *n*-alkane $\delta^{13}C$ values of C_3 plants are *c*. -36‰ VPDB (Vienna Pee Dee Belemnite) and *c*. -20‰ VPDB for C_4 plants (e.g. Diefendorf and Freimuth, 2017).

The hydrogen isotope composition of plant-waxes (δD_{wax}) reflects the isotopic composition of the water used during lipid biosynthesis (Sachse et al., 2012), rendering it a valuable tool for reconstructing past hydrological conditions (e.g. Collins et al., 2013; Schefuß et al., 2005). δD_{wax} is influenced by three main factors: i) the isotopic composition of precipitation; ii) enrichment of soil and leaf water due to ET; and iii) differences in the apparent isotopic fractionation between source water and plant-waxes due to differences in vegetation type. The importance of each factor varies by study site and with time. The detailed interpretation of the Mfabeni $\delta^{13}C_{wax}$ and δD_{wax} is discussed in section 6.1.

4. Methods: compound specific C and H isotope analyses

Core MF4-12 (6.96 m recovery, 8.77 m penetration) was recovered from the centre of Mfabeni peatland during January 2012 using a vibrocoring device (Fig. 2). The chronology of the core is established by 24 ^{14}C AMS (accelerator mass spectrometry) dates from bulk peat (Fig. 3, S1). The chronology is extended from that published in Humphries et al. (2017) and the age model is made using Bacon 2.2 program (Blaauw and Christen, 2011). Radiocarbon ages were calibrated using the southern hemisphere calibration curve, ShCal13 (Hogg et al., 2016) and post-bomb southern hemisphere curve, zone 1–2, for the uppermost modern dates (Hua et al., 2016).

Freeze-dried, bulk peat samples were ground and homogenized with a pestle and mortar, lipids were extracted from *c*. 2 g of peat with a DIONEX Accelerated Solvent Extractor (ASE 200) at 100 °C and at 1000 psi for 5 minutes (repeated 3 times) using a dichloromethane (DCM):methanol (MeOH) (9:1, v/v) mixture. Squalane was added prior to extraction as an internal standard. Elemental sulfur was removed from the TLEs using copper turnings, and water was removed by passing over a Na_2SO_4 column, eluting with hexane. After saponification, by adding 6 % KOH in MeOH, and extraction of the neutral fractions with hexane, the neutral fractions were split into hydrocarbon, ketone, and polar fractions using silica gel column chromatography (with a mesh size of 60 µm) and elution with hexane, DCM and DCM:MeOH (1:1), respectively. Subsequent elution with hexane over $AgNO_3$-impregnated silica columns obtained the saturated hydrocarbon fractions from the hydrocarbon fractions. The concentrations of long-chain *n*-alkanes in the saturated hydrocarbon fractions were measured using a Thermo Fischer Scientific Focus gas-chromatograph (GC) with flame-ionization-detection (FID) equipped with a Restek Rxi 5ms column (30 m x 0.25 mm x 0.25 µm). The split/splitless inlet temperature was 260 °C, the GC oven temperature was programmed at 60 °C, held for 2 min, increased at 20 °C/min to 150 °C and then at 4 °C/min to 320 °C and held for 11 minutes. Concentrations for isotope analyses were estimated by comparison with an external standard containing *n*-alkanes (C_{19}–C_{34}) at a concentration of 10 ng/µl that was run every 5 samples. Replicate analyses of the external standard yielded a quantification uncertainty of <5%.

The $\delta^{13}C$ values of the long-chain *n*-alkanes were measured using a Thermo Trace GC Ultra equipped with an Agilent DB-5 column (30m x 0.25mm x 0.25µm) coupled to a Finnigan MAT 252 isotope ratio monitoring mass spectrometer via a combustion interface operated at 1000 °C. The GC temperature was programmed from 120 °C (hold time: 3 min), followed by heating at 5 °C/min to 320 °C (hold time: 15 min). The $\delta^{13}C$ values were calibrated against external CO_2 reference gas and are reported in ‰ VPDB. Samples were analysed in duplicate when *n*-alkane concentrations were adequate for multiple runs. The internal standard (squalane, $\delta^{13}C$= -19.9‰), yielded an accuracy of 0.6‰ and a precision of 0.2‰ (n=37). The external standard mixture was analysed every 6 runs. The long-term precision and accuracy of the external *n*-alkane standard was 0.2 and 0.15‰, respectively. For $\delta^{13}C$ the average precision of the *n*-C_{29} and *n*-C_{31} alkane in replicates was 0.2‰ and 0.1‰ (n=22), respectively.

The δD compositions of long-chain *n*-alkanes were measured using a Thermo Trace GC coupled via a pyrolysis reactor (operated at 1420 °C) to a Thermo Fisher MAT 253 isotope ratio mass spectrometer (GC/IR-MS). The GC column and temperature program was similar to the $\delta^{13}C$ analysis. The δD values were calibrated against external H_2 reference gas and are reported in ‰ VSMOW. The H^{3+} factor was monitored daily and fluctuated around 5.2 ppm nA^{-1} during analyses. An *n*-alkane standard of 16 externally calibrated alkanes was measured every sixth measurement. The long-term precision and accuracy of the external *n*-alkane standard was 2.7 and 2‰, respectively. Samples were analysed in duplicate when *n*-alkane concentrations were adequate for multiple runs. The internal standard (squalane, δD= -180‰; ±2), yielded an accuracy of 0.9‰ and a precision of 1.9‰ (n=36). For δD the average precision in replicates was 1‰ for both *n*-C_{29} and *n*-C_{31} alkanes (n=52).

Last glacial Mfabani δD_{wax} values were corrected to account for the effect of changes in global ice volume (Collins et al., 2013; Schefuß et al., 2005). For this the benthic foraminifera-based oxygen isotope curve (Waelbroeck et al., 2002) was interpolated to each sample age and then converted to δD values using the global meteoric water line (Craig, 1961).

5. Results

This study focusses on the last 32 ka BP (*c*. 590 cm). The average temporal resolution between the 62 samples analysed for $\delta^{13}C$ and δD is *c*. 500 years. From 590 cm (32 ka BP) to 70 cm (*c*. 2 ka BP) the core is very dark brown in colour containing peat with humus, fine detritus and silt. From 70 cm to core top, the sediments are similar in colour to the peat below and contain fibrous peat with humus and herbaceous fine detritus (Humphries et al., 2017). Between 457 and 358 cm (*c*. 23–14 ka BP; comprising the LGM) mean grain sizes average at 110 µm, with smaller diameters averaging at 50 µm between 298 and core top (*c*. 11 ka–present, Holocene; Fig. 4g). The lithology of core MF4-12 does not exactly match with that observed from core SL6 (Baker et al., 2014; 2016; 2017), although sandy peat is observed during the LGM at both locations. This result is not surprising, multiple cores taken in transects across the bog indicate peat heterogeneity (Grundling et al., 2013).

Long chain *n*-alkane CPI values are generally around 6 (ranging from 2–13), indicating good *n*-alkane preservation. The two samples with CPI values of 2, potentially containing more degraded *n*-alkanes, are highlighted in red (Fig. 4b & c; Fig. 5b & c; Fig. 6). However, the in- or exclusion of these samples does not affect the observed pattern of changes and we thus consider the record to be suitable for palaeoclimate reconstruction. The samples contain *n*-alkanes with carbon chain lengths ranging from C_{17}–C_{35}, with C_{29} and C_{31} having the highest abundance. The high abundances of C_{29} and C_{31} enabled reliable isotopic analyses. The relationship between the δD and $\delta^{13}C$ of the C_{29} and C_{31} *n*-alkanes is strong, with R^2 values of 0.8 and 0.9, respectively. Consequently, for the $\delta^{13}C_{wax}$ and δD_{wax}, we use the amount-weighted mean of the C_{29} and C_{31} *n*-alkanes.

The $\delta^{13}C_{wax}$ values range from -29‰ to -21‰ (Fig. 4b). The ice volume δD correction decreases the glacial Mfabeni δD_{wax} values by <8 ‰ (Fig. 4c). The ice-corrected δD_{wax} values of the *n*-C_{29} and *n*-C_{31} alkanes range from -181‰ to -128‰ (Fig. 4c). P_{aq} values range from 0.02–0.7, averaging at 0.2 (Fig. 4f).

During the LGM (26.5–19 ka BP; Clark et al., 2009), $\delta^{13}C_{wax}$ and δD_{wax} values are relatively high averaging at -23‰ and *c*. -136‰, respectively (Fig. 4b & c) and P_{aq} values are low (*c*. 0.24; Fig. 4f). At *c*. 19 ka BP a 4‰ negative shift in $\delta^{13}C_{wax}$ values occurs (Fig. 4b). This negative shift in $\delta^{13}C_{wax}$ is concurrent with a gradual shift to lower δD_{wax} values (Fig. 4c) and an increase in P_{aq} values (Fig. 4f). Between 14 and 5 ka BP, $\delta^{13}C_{wax}$ values are relatively stable and average at -28‰ (Fig. 4b). δD_{wax} values become gradually lower during this period reaching -173‰ at 7.5 ka BP. At 5 ka BP, δD_{wax} values shift towards more positive values by 16‰ (Fig. 4c). Relatively high P_{aq} values occur between 14–5 ka BP (Fig. 4f). After *c*. 5 ka BP several high amplitude millennial-scale fluctuations in both $\delta^{13}C_{wax}$ and δD_{wax} values are evident. These fluctuations interrupt a trend where the isotope values of both $\delta^{13}C_{wax}$ and δD_{wax} gradually increase towards present day. A pronounced shift to higher $\delta^{13}C_{wax}$ and δD_{wax} values occurs at 2.8 ka BP. From *c*. 900 yr BP, $\delta^{13}C_{wax}$ and δD_{wax} values become higher reaching core top values of -21 and -128‰, respectively (Fig. 4b and c). Generally high, but variable and rapidly fluctuating P_{aq} values are evident between *c*. 5–0 ka BP. P_{aq} values decrease substantially after 1.3 ka BP from 0.6 to a core top value of *c*. 0 (Fig. 4f).

6. Discussion

6.1 Interpretation of the proxy signals

The relatively high CPI_{27-33} values indicate that the long-chain *n*-alkanes within the peat are derived from terrestrial higher plants and are relatively non-degraded. The long-chain *n*-alkanes are likely sourced directly from the local vegetation surrounding the coring location. It is possible that during times of stronger wind strength (i.e. during the LGM; Humphries et al., 2017) aeolian transport resulted in a higher biomarker contribution from more distal sources (i.e. the surrounding dune vegetation). Good preservation of *n*-alkanes in Mfabeni peat was also observed in nearby core SL6, but this was based on a CPI calculated using *n*-C_{21-31} (Baker et al., 2016). No relationship exists between the CPI and P_{aq} (R^2 = 0.11), this suggests that CPI variations at the location of core MF4-12 are not related to changes in organic matter preservation due to water table level variations.

The main source of carbon for terrestrial higher plants (the source of the C_{29} and C_{31} *n*-alkanes) is atmospheric CO_2, whereas aquatics also assimilate dissolved carbon, complicating the interpretation of their carbon isotope signal. We thus focus solely on C_{29} and C_{31} *n*-alkanes that are predominantly derived from terrestrial plants (Eglinton and Hamilton, 1967). The majority of the samples (67 %) have dominant *n*-alkane chain lengths of C_{29} and C_{31}. For the remaining 33 % of the samples, concentrated between 6 and 1.1 ka BP, the dominant chain length switched to *n*-C_{25}, indicating a higher *n*-alkane input from submerged macrophytes (Ficken et al., 2000). The *n*-C_{25} are unlikely to be sourced from mosses, as mosses are rare in subtropical peatland environments (Baker et al., 2016). Instead, the C_{25} is likely mainly derived from aquatic plants, which produce mid-chain *n*-alkanes as dominant homologues (C_{20}–C_{25}; Ficken et al., 2000). This increase of *n*-alkanes sourced from aquatic plants *c*. 6–1.1 ka BP is unlikely to have had any impact on the isotopic composition of the long-chain *n*-alkanes (C_{29} and C_{31}) as these are minor components in aquatic plants (e.g. Aichner et al., 2010). Therefore, we interpret the $\delta^{13}C_{wax}$ as changes in the C_3/C_4 ratio of terrestrial higher plants.

C_4 grasses are dominant within the SRZ, with C_3 grasses more prevalent in the WRZ at higher altitudes (Vogel et al., 1978). Previous palynological studies indicate that the dominant components of the pollen assemblage at Mfabeni are Poaceae and Cyperaceae (Finch and Hill, 2008). Although Cyperaceae species can be either C_3 or C_4, most Cyperaceae in eastern South Africa (67 %) are of the C_4-type (Stock et al., 2004). The C_4 vegetation at Mfabeni is thus mostly Poaceae or Cyperaceae from the sedge and reed fen. The C_3 vegetation at Mfabeni is comprised of arboreal taxa from the swamp forest (e.g. Myrtaceae and *Ficus*) and locally distributed *Podocarpus* (Finch and Hill, 2008; Venter, 2003). Shifts to heavier $\delta^{13}C_{wax}$ values (more C_4-type vegetation) at Mfabeni could indicate an expansion of grassland, as a result of either: i) colder conditions, ii) lesser precipitation provided by the tropical easterlies (weaker summer rains), iii) a longer/more intense dry season, iv) heightened ET, v) reduced water table height, or vi) reduced atmospheric CO_2 (or any combination of the above).

The δD_{wax} reflects the δD_{precip}, ET amount and vegetation type. The δD_{precip} can be influenced by changes in air temperature, with an estimated temperature effect of *c*. 0.5‰ per 1°C for $\delta^{18}O_{precip}$ (Dansgaard, 1964). The estimated temperature change of *c*. 2 °C at Mfabeni from the LGM to Holocene (Chevalier and Chase, 2015), would thus correspond to a change in $\delta^{18}O_{precip}$ of 1‰. Conversion to changes in δD_{precip} using the global meteoric water line would thus lead to a potential LGM to Holocene δD_{precip} enrichment of 8‰ (Craig, 1961). However, the Mfabeni δD_{wax} record shows a depletion in δD_{wax} from the LGM to the Holocene, rather than an enrichment. The observed glacial δD depletion is therefore a conservative estimate. Consequently, changes in temperature from the LGM to the Holocene did not exert a dominant control on Mfabeni δD_{wax}.

Changes in vegetation type (C_3/C_4) have the potential to reduce or exaggerate shifts in δD_{wax}. There are differences in the apparent fractionation (the integrated isotopic fractionation between precipitation and plant-wax lipids) between plant types using different photosynthetic pathways. C_3-type shrubs and trees fractionate the least, C_4-type grasses slightly more, while C_3-type grasses show the highest apparent fractionation (Sachse et al., 2012). This relationship occurs due to physiological differences, with grasses monocotyledonous and shrubs and trees dicotyledonous. Nevertheless, recent data suggest that the effect of C_3-tree to C_4-grass vegetation type changes on δD_{wax} likely is relatively small (Collins et al., 2013; Vogts et al., 2016). Therefore, the observed variability in δD_{wax} at Mfabeni is most likely the result of relative changes in the amount of ET versus changes in precipitation.

During times of heightened ET and/or lower precipitation amount, soil waters become enriched in D (e.g. Sprenger et al., 2017). Furthermore, under conditions of low ambient relative humidity, leaf water becomes enriched in D through increased transpiration (Kahmen et al., 2013). Mfabeni has high rates of ET, which can equal, or even exceed precipitation during dry periods (Grundling et al., 2015). ET is therefore likely a dominant factor controlling the enrichment of D within soil and leaf waters, and consequently in leaf waxes at Mfabeni.

High δD_{wax} values at Mfabeni likely result from decreased summer precipitation amount and/or heightened ET. Studies investigating the present-day relationship between precipitation amount and δD indicate 'extreme' shifts by up to 15‰ with the passage of the ITCZ, 7‰ with the passage of convective storms or around 1.5‰/100 mm of monthly precipitation (Gat et al., 2001). Much larger values of isotopic enrichment (*c*. 55‰) are associated with the effects of evaporation (Kim and Lee, 2011). The large isotopic variability observed within the Mfabeni record (*c*. 53‰) therefore implies that both changes in precipitation and ET amount are needed to explain the δD_{wax} variability over the past 32 ka BP. The similarity between the δD_{wax} pattern and the regional precipitation/aridity stacks (Chevalier and Chase, 2015; 2016) support this inference and indicate that the hydrological fluctuations in the Mfabeni record represent hydrological change at a broader spatial scale (Fig. 4c–e), but also suggest that the pollen-based precipitation stacks may also include an element of ET variability.

6.2 Climatic and environmental conditions at Mfabeni over the last 32 ka BP

The $\delta^{13}C_{wax}$, δD_{wax} and P_{aq} data from Mfabeni indicate that the vegetation, hydrology and the water table varied considerably over the last 32 ka BP (Fig. 4 & Fig. 5). The high $\delta^{13}C_{wax}$ values during the LGM indicate that the vegetation was likely dominated by more drought-tolerant C_4 plant types (Fig. 4b). Similar LGM $\delta^{13}C_{wax}$ depletion was observed previously at Mfabeni (Fig. 4h; Baker et al., 2017). Drier conditions during the LGM are also consistent with the observed low P_{aq} values that indicate a higher relative contribution of terrestrial-over-aquatic *n*-alkanes, likely a consequence of a lower water table (Fig. 4f). The high δD_{wax} values during the LGM suggest decreased summer precipitation and/or higher ET amount, which are both consistent with a drier environment (Fig. 4c). We cannot completely rule out the possible impact of increased drainage of the peatbog during the LGM due to low eustatic sea level (Grundling et al., 2013), however, the fact that the peat continued to grow during the LGM suggests that the sea level effect was minor. Indeed, the organic geochemical proxies agree with palynological data indicating regional grassland dominance (high Poaceae, Cyperaceae and Asteraceae) with low amounts of arboreal taxa (Fig. 6; Finch and Hill, 2008). Regional aridity and/or stronger wind strength are also indicated by increased grain size of the lithogenic sediment fraction at Mfabeni (Fig. 4g; Humphries et al., 2017). The dry conditions at Mfabeni during the LGM appear to be part of a wider eastern South African pattern, since they are consistent with regional precipitation and the aridity stacks (Fig. 4d & e).

The shift to more negative $\delta^{13}C_{wax}$ values following the LGM, at *c*. 19 ka BP, indicating that the vegetation at Mfabeni changed to more C_3-type plants (Fig. 4b), is also evident in Mfabeni core SL6 (Fig. 4h; Baker et al., 2017). This change is thus representative of C_3/C_4 changes across the peat bog. However, the palynological record indicates no shift towards arboreal taxa at this time but instead a continuation of grasslands (Fig. 6; Finch and Hill, 2008). Baker et al. (2017) suggested that this carbon isotope shift resulted from the increase in temperature across the glacial-interglacial transition. However, higher growing-season temperatures would favour C_4 over C_3 grasses (Ehleringer, 1997) and we therefore suggest that the carbon isotope decrease represents a shift from C_4 grasses to C_3 grasses (or from C_4 sedges to C_3 sedges).

After *c*. 19 ka, the $\delta^{13}C_{wax}$ values continue to decrease to -29‰ until they plateau at *c*. 14 ka BP, indicating continued expansion of C_3 vegetation. This trend in $\delta^{13}C_{wax}$ values between *c*. 19 and 14 ka BP corresponds well with a decrease in aeolian dust (Humphries et al., 2017) and the $\delta^{13}C_{wax}$ record from Mfabeni core SL6 (Baker *et al.*, 2017; Fig. 4b & 4h). There are, however, some minor differences between the two $\delta^{13}C_{wax}$ records. We attribute these to small-scale variations in vegetation across the peatbog, the lower sampling resolution of core SL6 and to dating uncertainties in both records. The shift to lower $\delta^{13}C_{wax}$ values at 19 ka BP occurs at the same time as a rise in the water table as documented by an increase in P_{aq} values (Fig. 4f). The gradual shift to lower δD_{wax} values around 19 ka BP occurs during decreasing local summer insolation, suggesting that this moisture shift was unlikely to be a result of increased precipitation, but more likely resulting from lower ET rates due to decreasing wind strength.

The $\delta^{13}C_{wax}$ values between 14–5 ka BP reflect a stable period of C_3-type vegetation (Fig. 4b). At the same time, gradually decreasing δD_{wax} values indicate increasing humidity. Pollen data from Mfabeni provide evidence for an expansion of arboreal type vegetation at *c.* 12 ka BP (Fig. 6; Finch and Hill, 2008). The pollen data thus suggest the establishment of swamp forest vegetation during the early Holocene, indicative of a moist climate (Fig. 6). Mfabeni aeolian sediment grain size are low and stable throughout this period, also suggesting a moist climate and low wind strength (Fig. 4g). The moist climate likely resulted in vegetated dunes, reducing the amount of material available for aeolian transport. The relatively high P_{aq} values between 14–5 ka BP indicate a high and stable water table at this time (Fig. 4f). Elevated total organic carbon percentages within Mfabeni core SL6 during the Holocene, also suggest increased water levels (Baker et al., 2017).

Between *c.* 5–0 ka BP several high-amplitude millennial-scale C_3/C_4 vegetation changes are evident superimposed on an overall shift from predominantly C_3 to more C_4-type vegetation towards the present-day (Fig. 5b). This variability contrasts with the more gradual C_4/C_3 vegetation transition from the Glacial to Holocene. The $\delta^{13}C_{wax}$ values from Mfabeni core SL6 between *c.* 6–1 ka BP also indicate a period of predominantly C_4-type vegetation, implying arid conditions during this time (Baker et al., 2017; Fig. 4h). A similar pattern of a long-term trend with superimposed short-term variability is visible in the in δD_{wax} record. The general enrichment in D reflects gradual drying, punctuated by millennial-scale pulses of aridity, with the most pronounced arid event at *c.* 2.8 ka BP (Fig. 5c). Counterintuitively, the high abundance of *n*-C_{25} alkanes and high but variable P_{aq} values between *c.* 5–0 ka BP indicate a generally high water table, interrupted by brief periods of a lower water table (Fig. 5d). After 2.3 ka BP, both $\delta^{13}C_{wax}$ and δD_{wax} values become higher and P_{aq} values lower (Fig. 5b–d). This suggests increased C_4-type vegetation cover, decreased summer precipitation and/or higher ET amount and low water table levels. The increased variability between 5–0 ka BP could be an artefact of the high temporal resolution of our record during this interval (~220 vs ~700 years per sample for the remainder of the record). Nevertheless, other data from the region (e.g. Baker et al., 2017, Humphries et al., 2017; 2016, Finch and Hill, 2008, Neumann et al., 2010) also indicate climatic instability and pulses of arid climatic conditions during the last *c*. 5 ka BP, suggesting that the observed variability is real (Fig. 5e). The long-term drying trend is unlikely to be caused by decreased summer precipitation because local summer insolation and Mozambique Channel SSTs are high (Fig. 5a & Fig. 4j). Instead, the general drying trend is more likely a result of heightened ET during the late Holocene.

6.3 Climate driving mechanisms

Modern observations suggest that warm SSTs within the Mozambique Channel and Agulhas Current induce increased evaporation (e.g. Walker, 1990), resulting in increased onshore airflow and advection of moist air and higher rainfall in the SRZ (Tyson, 1999). Variations in local SST are thus thought to be an important driver of hydroclimate in eastern South Africa. This mechanism may also play a key role on longer time scales. Indeed, Chevalier and Chase (2015) mention this hypothesis, invoking SSTs as the dominant driver of precipitation variability during the LGM, and Baker et al. (2017) argue for the existence of a short arid event at 7.1 ka BP that corresponds to a decrease in Mozambique Channel SSTs. However, Mfabeni vegetation and hydrology reconstructions over the last 32 ka BP do not show a close relationship with changes in southwest Indian Ocean SSTs (Fig. 4j, Wang et al., 2013). This suggests that SST variability is unlikely to be the sole driver of the changes in hydroclimate at Mfabeni over the 32 ka. Thus, we suggest an additional role, namely the southern hemisphere westerlies.

We attribute the arid climate and the associated expansion of drought tolerant C_4 plants and a low water table at Mfabeni during the LGM, in part, to a northward displacement of the southern hemisphere westerly winds, shifting the hydroclimate to a more evaporative regime, where ET exceeds precipitation. In addition, lower SSTs (Fig. 4j) in the Mozambique Channel at this time likely reduced moisture availability. It is possible that the combination of a northward displacement of the southern hemisphere westerlies and lower SSTs shifted the fine balance between precipitation and ET at Mfabeni towards higher ET rates during the LGM.

Numerous palaeoenvironmental studies (e.g. Lamy et al., 2001; Lamy et al., 2010; Stuut and Lamy, 2004; Chase et al., 2017) and climate model simulations (e.g. Cockcroft et al., 1987; Rojas et al., 2009; Toggweiler et al., 2006), indicate an intensification and equatorward migration of the southern hemisphere westerlies in response to the increased extent of Antarctic sea ice during the LGM. Such changes may have expanded the limit of the WRZ in South Africa northward, to around 25°S in the west and 30°S in the east (Cockcroft et al., 1987). This would have put Mfabeni (at 28°S) within the range of the southern westerlies. Regions on the east coast, such as Mfabeni, then experienced stronger winter winds, causing heightened ET (Humphries et al., 2017). With more northerly westerlies, the duration of the dry season at Mfabeni may also have been extended diminishing the influence of the easterlies. This shortened the rain season and heightened ET rates. The northward

Clim. Past Discuss., https://doi.org/10.5194/cp-2019-4
Manuscript under review for journal Clim. Past
Discussion started: 21 January 2019

shift in the westerlies during the LGM is also visible in records from the present WRZ (e.g. Chase et al., 2017), which show increased winter rainfall and moist conditions (Fig. 4i).

Although during the LGM the southern hemisphere westerlies were in a more northerly position and had the potential to provide rainfall, we do not see any evidence that the source of precipitation changed. Today the moisture at Mfabeni is mainly provided by the tropical easterlies (Kruger et al., 2010; Tyson, 1999), and thus we see enriched D values on the east coast and more depleted values further inland (δD_{precip} data from GNIP (IAEA, 2018) and groundwater δD data from West et al., 2014). Precipitation sourced from the southern hemisphere westerlies would be strongly depleted in D because of the large continental transport distance from the Atlantic Ocean. However, there is no evidence of lower δD_{wax} values during the LGM at Mfabeni, indicating the westerlies did not bring moisture to Mfabeni during the LGM but that increased wind strength led to increased ET and a more arid climate.

We suggest that the shift to more humid conditions at *c*. 19 ka BP was related to the retreat of the southern hemisphere westerlies from this area as Antarctic sea ice began to retreat poleward at this time (Fig. 4k), leading to less ET and allowing an increased influence of the moist tropical easterlies. This shift was unlikely driven by a change in local summer insolation (i.e. Chevalier and Chase, 2015) because insolation was decreasing at this time, which would have caused reduced, instead of enhanced, summer precipitation. We suggest that the abrupt shift to more C_3 vegetation was a non-linear response to increasing moisture availability in the peatbog (Fig. 4c). Precipitation amount may have reached a critical threshold at *c*. 19 ka BP for the establishment of C_3 type vegetation, resulting in the observed abrupt vegetation shift (Fig. 4b). We propose that at *c*. 19 ka BP, the position of the southern westerlies had a greater climatic influence than the local insolation forcing. Further south, within the present WRZ, the retreat of the westerlies at this time resulted in a shift to more arid conditions (Fig. 4i; Chase et al., 2017). The timing of increased humidity at Mfabeni at *c*. 19 ka BP corresponds well to a reduction in Antarctic sea ice extent, which is thought to be the main driver of the latitudinal position of the westerlies (Fig. 4k; Fischer et al., 2007).

Between 14–5 ka, low Antarctic sea ice (Fig. 4k & 5g), resulted in a more poleward position of the westerlies. The diminished effect of the westerlies in eastern South Africa at this time permitted the tropical easterlies, and thus local summer insolation, to dominate the climatic regime at Mfabeni. Indeed, increasing humidity at Mfabeni at this time, corresponds with increasing southern hemisphere summer insolation (Fig. 4a). The importance of insolation for South African climate variability during the late Quaternary has been suggested before (e.g. Partridge et al., 1997; Simon et al., 2015; Schefuß et al., 2011; Chevalier and Chase, 2015). However, we suggest that direct local insolation forcing is only dominant when the westerlies are located far south.

After *c.* 5 ka BP, palaeoenvironmental records from the WRZ, such as from Verlorenvlei (Fig. 1; Fig. 5f; Carr et al., 2015), Seweweekspoort (Fig. 1; Fig. 4h; Chase et al., 2017), Klaarfontein (Fig. 1; Meadows and Baxter, 2001), Cecilia Cave (Fig. 1; Baxter, 1989) and Eilandvlei (Wündsch et al., 2018) document increased moisture supply to the WRZ, implying a recurring more northerly location of the westerly storm tracks at this time. Chevalier and Chase et al. (2015) propose that increased precipitation in the WRZ during the late Holocene was due to both the warmer interglacial climate and the northward expansion of the westerly storm tracks. Although no indication for an increase in sea ice is evident from EPICA salt concentration data (Fig. 4k), diatom data (*Fragilariopsis curta* and *F. cylindrus*) from PS2090/ODP1094 in the southern South Atlantic document an increase in sea ice during the late Holocene (Fig. 5g), which may have pushed the southern westerlies equatorward. In addition, climate modelling results imply a northward shift of the southern hemisphere westerlies at this time (Hudson and Hewitson, 2001). Consequently, in a comparable way to the LGM, the increased sea ice during the late Holocene (Fig. 5g), may have displaced the westerlies equatorward, increasing winter wind strength and the length of the dry season at Mfabeni, leading to a decreased influence of the moisture bearing tropical easterlies (Mejía et al., 2014; Toggweiler et al., 2006; Williams and Bryan, 2006). Furthermore, although the westerlies may have had a more northerly position during this time, simultaneous high local summer insolation and warm SSTs (causing strong convective rainfall during summer; Fig. 5a) may have been the cause of the relatively high water table (Fig. 5d) and transitory peaks in precipitation and C_3-type vegetation expansion (Fig. 5b and c). Interestingly, the hydrological variability at Mfabeni (Fig. 5c) during the last *c.* 5 ka BP, is not present in the central and eastern South African precipitation stack (Fig. 4d). We attribute this to the highly sensitive balance between ET and precipitation at Mfabeni (Grundling et al., 2015), and the fact that the precipitation stack smoothes local hydrological variability.

It is possible that anthropogenic influences also played a role in shaping the environment at Mfabeni during, at least, during the late Holocene. However, unequivocal agricultural and exotic pollen indicators are absent from the pollen record and although pollen data indicate that deforestation occurred during the late Holocene, it is unclear whether this was related to human influence or regional climatic change (Finch and Hill, 2008). The deforestation could have affected the water table and increased the relative amount of C_4-type vegetation. The appearance of *Morella* and *Acacia* in the late Holocene may indicate the development of open vegetation or secondary forest due to fire disturbance (Finch and Hill, 2008). Human activities or climate change may be responsible for changes in fire regime. With no palaeo-charcoal data available for Mfabeni, no direct evidence for increased fire activity during the late Holocene exists. In addition, the palaeoenvironmental evidence available suggests that the arid conditions during the late Holocene were regional in nature (Scott, 1999; 2003; Humphries et al., 2016, Neumann et al., 2010). Thus, any human activity was unlikely the primary cause of the late Holocene regional aridity and the large magnitude of environmental changes observed at Mfabeni.

Today ENSO activity is one of the most important driving mechanisms for inter-annual climatic variability in South Africa (Tudhope et al., 2001). Southern Africa's seasonal rainfall is linked to ENSO, with dry (wet) conditions associated with El Niño (La Niña) events (Archer et al., 2017; Mason and Jury, 1997). According to the model of Tyson (1986), during El Niño events, high Indian Ocean SSTs produce a weaker landward pressure gradient over the southeast African coast, diminishing low-level confluence over the continent. This results in a longitudinal migration of the ascending limb of the Walker circulation eastwards, leading to lower rainfall on the continent (i.e at Mfabeni) but higher rainfall towards the east (i.e Madagascar; Mason and Jury, 1997). Furthermore, during El Niño events, a northward shift of the westerlies may occur, which could increase rainfall over western South Africa but lead to aridity in the east (i.e. at Mfabeni; Lindesay, 1988). Although after *c*. 5 ka BP the Mfabeni sampling resolution is higher, we document some evidence for heightened climatic variability (in comparison with the rest of the record) and generally drier conditions at Mfabeni over the last *c*. 5 ka BP. We speculate that this variability may have been the result of amplified ENSO activity (e.g. Humphries et al., 2017). Palaeoenvironmental studies in the Pacific Basin and South America indicate that during the early Holocene El Niño events were smaller and occurred less frequently, with a shift to stronger ENSO activity after *c*. 5 ka BP (Fig. 5h, Moy et al., 2002; Huffman, 2010; Rodbell et al., 1999; Sandweiss et al., 1996; Tudhope et al., 2001).

We therefore invoke a combination of both the northerly-displaced southern hemisphere westerlies and the impact of high ENSO variability as climatic drivers during the last *c*. 5 ka BP. The high-amplitude, millennial-scale vegetation and hydrological instability documented at Mfabeni during the last *c*. 5 ka BP contrasts with the relatively stable conditions during the LGM and early Holocene. This increased environmental variability during the late Holocene could be the result of increased and strongly fluctuating sea ice extent during this period, overlain by strong ENSO activity (Moy et al., 2002).

7. Conclusions

Compound specific carbon and hydrogen isotope data and *n*-alkane distributions (P_{aq}) from Mfabeni peatbog are used to reconstruct climatic conditions, over the last 32 ka BP, in eastern South Africa. The LGM at Mfabeni was characterized by a high contribution of C_4 grasses, high ET rates and a low water table. During the LGM increased Antarctic sea ice extent led to an equatorward displacement of the southern hemisphere westerly winds, which extended the length and increased the intensity of the dry season at Mfabeni. Between *c*. 19–5 ka BP an expansion of C_3-type vegetation occurred, with more rainfall and a higher water table at Mfabeni. At *c*. 19 ka BP, Antarctic sea ice decreased, which resulted in a southward retreat of the southern hemisphere westerlies. This southward retreat of the westerlies after *c.* 19 ka BP and an increase in local summer insolation after *c.* 12 ka BP resulted in more precipitation and increased wet season length at Mfabeni. When the westerlies were in their southernmost position (*c.* 14–5 ka BP), local insolation became the dominant control on Mfabeni climate, leading to stronger convection and enhanced monsoonal precipitation from the tropical easterlies. The late Holocene (*c.* <5 ka BP) was characterized by increased environmental instability and increasingly arid conditions. We attribute these trends to concurring high local summer insolation and the recurring influence of the southern westerlies and/or heighted ENSO activity.

The Mfabeni record indicates that climate and environmental variability in eastern South Africa over the last 32 ka BP is driven by a combination of i) enhanced/reduced moisture transport by the tropical easterlies, driven by variations in southern hemisphere summer insolation, and ii) latitudinal displacements of the southern hemisphere westerlies. With the expansion and retreat of Antarctic sea ice responsible for the displacement of the westerlies, we invoke high-latitude climate forcing as an important driver of climate in eastern South Africa.

Data availability: Supplementary data for age-model (S1) is available with this manuscript. Other data is available on PANGAEA.

Author contributions: CM and ES conducted $\delta^{13}C_{wax}$ and δD_{wax} analyses. Interpretation was carried out by CM, JF, TH, FP, MH, MZ and ES.

Competing interests: The authors declare no competing financial interests.

Acknowledgements: This research was funded by the Bundesministerium für Bildung und Forschung (BMBF; RAiN project 03G0840A/B) and NRF Grant 84431 (JF). We thank R. Kreutz for assistance with $\delta^{13}C_{wax}$ and δD_{wax} data acquisition and L. Jonkers for helpful input with manuscript writing.

Figure captions

Figure 1. a) Rainfall seasonality map for southern Africa showing the major oceanic and atmospheric currents, the position of the intertropical convergence zone (ITCZ) and the Congo Air Boundary (CAB). Red/orange = summer rainfall zone (SRZ). Green = year-round rainfall zone (YRZ). Blue is winter rainfall zone (WRZ). The white arrows are atmospheric circulation and the blue arrows are oceanic circulation. Map courtesy of B. Chase (Chase et al., 2017). Letters represent key study sites mentioned in the text (and shown in Fig. 4 and 5): **a)** GIK16160-3 (Wang et al., 2013). **b)** Mfabeni, this study. **c)** Lake St Lucia

(Humphries et al., 2016). **d)** Seweweekspoort (Chase et al., 2017). **e)** Cecilia Cave (Baxter, 1989). **f)** Klaarfontein (Meadows and Baxter, 2001) and Verlorenvlei, one location.

Figure 2. Mfabeni peatland and its regional geomorphological features, indicating the location of core MF4-12 (red circle, this study) and the location of core SL6 (black circle, Baker et al., 2014; 2016; 2017). Map is courtesy of B. Gijsbertsen, UKZN Cartography Unit.

Figure 3. Depth-age model of core MF4-12 produced using Bacon, based on 24 ^{14}C AMS dates. Blue symbols are AMS dates and grey shading indicates 95% confidence interval on the mean age (red line).

Figure 4. Climate and environmental change at Mfabeni compared with regional records and orbital insolation. **a**) December-January-February (DJF) insolation for 28°S (blue line; Laskar, 2011). **b**) Stable carbon isotope composition (weighted mean) of C_{29}–C_{31} *n*-alkanes from Mfabeni, reflecting changes in C_3/C_4 vegetation type. **c**) Hydrogen isotope composition (weighted mean) of C_{29}–C_{31} *n*-alkanes from Mfabeni, reflecting changes in summer precipitation and ET amount. Red is the δD_{wax} corrected for ice volume changes. Error bars on isotope data reflect analytical uncertainty of duplicate analyses. **d**) Central and eastern South African regional precipitation stack (red line; Chevalier and Chase, 2015). **e**) Southern African regional aridity stack (Chevalier and Chase, 2016). **f**) P_{aq} at Mfabeni, indicating the amount of aquatic vs. terrestrial *n*-alkanes (high/low water table). **g**) Mean grain size data of the lithogenic sediment fraction from Mfabeni, with increased grain size indicating increased wind strength (Humphries et al., 2017). **h)** Mfabeni core SL6 stable carbon isotope composition (weighted mean) of C_{29}–C_{31} *n*-alkanes (Baker et al., 2017). **i)** Combined nitrogen isotope data from Seweweekspoort rock hyrax middens, reflecting changes in humidity (Chase et al., 2017). **j**) $U^{K'}_{37}$ derived SSTs from core GIK16160-3 in the Mozambique Channel (Wang et al., 2013). **k**) Sea salt sodium concentrations from the EPICA DML ice core in Antarctica, reflecting changes in sea ice coverage (Fischer et al., 2007). The two Mfabeni samples with CPI values of *c*. 2 are highlighted in red (4b & c). SHW = southern hemisphere westerlies. Blue shading = Mfabeni wet, orange = Mfabeni arid.

Figure 5. Comparison of Mfabeni data with other records of environmental variability over the last 15 ka BP. a) DJF insolation for 28°S (black line; Laskar, 2011). b) Carbon isotope composition (weighted mean) of C_{29}–C_{31} *n*-alkanes from Mfabeni, reflecting changes in C_3/C_4 vegetation type. c) Hydrogen isotope composition (weighted mean) of C_{29}–C_{31} *n*-alkanes from Mfabeni, reflecting changes in summer precipitation and ET amount. d) P_{aq} at Mfabeni, indicating the amount of aquatic vs. terrestrial n-alkanes (high/low water table). Blue dashed lines highlight trends. e) Mfabeni calcium/scandium ratio, indicating changes in water table (Humphries et al., 2017). f) Bulk carbon isotope data from

Verlorenvlei (Carr et al., 2015). g) Extent of Antarctic sea ice. Estimation is based on the abundance of *Fragilariopsis curta* and *Fragilariopsis cylindrus* at site PS2090/ODP1094 (SW of Cape Town; Bianchi and Gersonde, 2004). h) Red colour intensity time-series from Laguna Pallcacocha. High values are light coloured inorganic clastic laminae, which were deposited during ENSO-driven episodes (Moy et al., 2002). The Mfabeni sample with a CPI value of *c*. 2 is highlighted in red (5b & c).

Figure 6. Summary figure highlighting the main climate phases and driving mechanisms at Mfabeni. From left: hydrogen isotope composition (weighted mean) of C_{29}–C_{31} *n*-alkanes from Mfabeni. Red is the δD_{wax} corrected for ice volume changes. Stable carbon isotopic composition (weighted mean) of C_{29}–C_{31} *n*-alkanes from Mfabeni. The two Mfabeni samples with CPI values of *c*. 2 are highlighted in red. Summary of the palynological data from Finch and Hill (2008) and possible climate driving mechanisms at Mfabeni during the last 32 ka BP.

References

Archer, E.R.M., Landman, W.A., Tadross, M.A., Malherbe, J., Weepener, H., Maluleke, P., Marumbwa, F.M.: Understanding the evolution of the 2014–2016 summer rainfall seasons in southern Africa: Key lessons, Climate Risk Management, 16, 22-28, 2017.

Aichner, B., Herzschuh, U., Wilkes, H.: Influence of aquatic macrophytes on the stable carbon isotopic signatures of sedimentary organic matter in lakes on the Tibetan Plateau, Org. Geochem., 41, 706-718, 2010.

Baker, A., Routh, J., Blaauw, M., Roychoudhury, A.N.: Geochemical records of palaeoenvironmental controls on peat forming processes in the Mfabeni peatland, Kwazulu Natal, South Africa since the Late Pleistocene, Palaeogeogr. Palaeoecol., 395, 95-106, 2014.

Baker, A., Routh, J., Roychoudhury, A.N.: Biomarker records of palaeoenvironmental variations in subtropical Southern Africa since the late Pleistocene: Evidences from a coastal peatland, Pleistocene. Palaeogeogr. Palaeoecol., 451, 1-12, 2016.

Baker, A., Pedentchouk, N., Routh, J., Roychoudhury, A.N.: 2017. Climatic variability in Mfabeni peatlands (South Africa) since the late Pleistocene, Quaternary Sci.Rev., 160, 57-66, 2017.

Barker, P.A., Leng, M.J., Gasse, F., Huang, Y.: Century-to-millennial scale climatic variability in Lake Malawi revealed by isotope records, Earth Planet. Sci.Lett., 261, 93-103, 2007.

Baxter, A.J.: Pollen analysis of a Table Mountain cave deposit. University of Cape Town, Cape Town. 1989.

Bianchi, C., Gersonde, R.: Climate evolution at the last deglaciation: the role of the Southern Ocean, Earth Planet. Sci.Lett., 228, 407-424, 2004.

Blaauw, M., Christen, J.A.: Flexible paleoclimate age-depth models using an autoregressive gamma process, Bayesian Anal., 6, 457-474, 2011.

Burdanowitz, N., Dupont, L., Zabel, M., Schefuß, E.: Holocene hydrologic and vegetation developments in the Orange River catchment (South Africa) and their controls, The Holocene, 2018.

Braconnot, P., Otto-Bliesner, B., Harrison, S., Joussaume, S., Peterchmitt, J.Y., Abe-Ouchi, A., Crucifix, M., Driesschaert, E., Fichefet, T., Hewitt, C.D., Kageyama, M., Kitoh, A., Laîné, A., Loutre, M.F., Marti, O., Merkel, U., Ramstein, G., Valdes, P., Weber, S.L., Yu, Y., Zhao, Y.: Results of PMIP2 coupled simulations of the Mid-Holocene and Last Glacial Maximum – Part 1: experiments and large-scale features, Clim. Past, 3, 261-277, 2007.

Bray, E.E., Evans, E.D.: Distribution of n-paraffins as a clue to recognition of source beds, Geochim. et Cosmochim. Ac., 22, 2-15, 1961.

Carr, A.S., Boom, A., Chase, B.M.: Meadows, M.E., Grimes, H.L.: Holocene sea level and environmental change on the west coast of South Africa: evidence from plant biomarkers, stable isotopes and pollen, J. Paleolimnol., 53, 415-432, 2015.

Chase, B.M., Chevalier, M., Boom, A., Carr, A.S.: The dynamic relationship between temperate and tropical circulation systems across South Africa since the last glacial maximum, Quaternary Sci.Rev., 174, 54-62, 2017.

Chase, B.M., Lim, S., Chevalier, M., Boom, A., Carr, A.S., Meadows, M.E., Reimer, P.J.: Influence of tropical easterlies in southern Africa's winter rainfall zone during the Holocene, Quaternary Sci.Rev., 107, 138-148, 2015.

Chase, B.M., Meadows, M.E.: Late Quaternary dynamics of southern Africa's winter rainfall zone, Earth-Sci. Rev., 84, 103-138, 2007.

Chevalier, M., Chase, B.M.: Southeast African records reveal a coherent shift from high- to low-latitude forcing mechanisms along the east African margin across last glacial–interglacial transition, Quaternary Sci.Rev., 125, 117-130, 2015.

Chevalier, M., Chase, B.M.: Determining the drivers of long-term aridity variability: a southern African case study. J. Quaternary Sci., 31, 143-151, 2016.

Clark, P.U., Dyke, A.S., Shakun, J.D., Carlson, A.E., Clark, J., Wohlfarth, B., Mitrovica, J.X., Hostetler, S.W., McCabe, A.M.: The Last Glacial Maximum, Sci. J., 325, 710-714, 2009.

Cockcroft, M.J., Wilkinson, M.J., Tyson, P.D.: The application of a present-day climatic model to the late quaternary in southern Africa. Clim. Change, 10, 161-181, 1987.

Collins, J.A., Schefuß, E., Mulitza, S., Prange, M., Werner, M., Tharammal, T., Paul, A., Wefer, G.: Estimating the hydrogen isotopic composition of past precipitation using leaf-waxes from western Africa, Quaternary Sci.Rev., 65, 88-101, 2013.

Collister, J.W., Rieley, G., Stern, B., Eglinton, G., Fry, B.: Compound-specific δ 13C analyses of leaf lipids from plants with differing carbon dioxide metabolisms. Org. Geochem., 21, 619-627, 1994.

Craig, H., Isotopic Variations in Meteoric Waters, Sci. J., 133, 1702-1703. 1961.

Dansgaard, W.: Stable isotopes in precipitation, Tellus, 16, 436-468, 1964.

Diefendorf, A.F., Freimuth, E.J.: Extracting the most from terrestrial plant-derived n-alkyl lipids and their carbon isotopes from the sedimentary record: A review, Org. Geochem., 103, 1-21. 2017.

Dupont, L., Caley, T., Kim, J.-H., Castañeda, I.S., Malaizé, B., Giraudeau, J.: Glacial-interglacial vegetation dynamics in South Eastern Africa coupled to sea surface temperature variations in the Western Indian Ocean, Clim. Past 7, 1209-1224, 2011.

Dupont, L.: Orbital scale vegetation change in Africa, Quaternary Sci.Rev., 30, 3589-3602, 2011.

Eglinton, G., Hamilton, R.J.: Leaf Epicuticular Waxes, Sci. J., 156, 1322-1335, 1967.

Ehleringer, J.R.: C4 photosynthesis, atmospheric CO2, and climate, Oecologia 112, 285-299, 1997.

Ficken, K.J., Li, B., Swain, D.L., Eglinton, G.: An n-alkane proxy for the sedimentary input of submerged/floating freshwater aquatic macrophytes, Org. Geochem., 31, 745-749, 2000.

Finch, J.M., Hill, T.R.: A late Quaternary pollen sequence from Mfabeni Peatland, South Africa: Reconstructing forest history in Maputaland. Quaternary Res., 70, 442-450, 2008.

Fischer, H., Fundel, F., Ruth, U., Twarloh, B., Wegner, A., Udisti, R., Becagli, S., Castellano, E., Morganti, A., Severi, M., Wolff, E., Littot, G., Röthlisberger, R., Mulvaney, R., Hutterli, M.A., Kaufmann, P., Federer, U., Lambert, F., Bigler, M., Hansson, M., Jonsell, U., de Angelis, M., Boutron, C., Siggaard-Andersen, M.-L., Steffensen, J.P., Barbante, C., Gaspari, V., Gabrielli, P., Wagenbach, D.: Reconstruction of millennial changes in dust emission, transport and regional sea ice coverage using the deep EPICA ice cores from the Atlantic and Indian Ocean sector of Antarctica, Earth Planet. Sci. Lett., 260, 340-354. 2007.

Gat, J.R., Mook, W.G., Meijer, H.A.: Environmental isotopes in the hydrological cycle, Water Resources Programme, 2001.

Grundling, P., Clulow, A.D., Price, J.S., Everson, C.S.: Quantifying the water balance of Mfabeni Mire (iSimangaliso Wetland Park, South Africa) to understand its importance, functioning and vulnerability, Mires Peat, 16, 1-18, 2015.

Grundling, P., Grootjans, A.P., Price, J.S., Ellery, W.N., Development and persistence of an African mire: How the oldest South African fen has survived in a marginal climate, CATENA, 110, 176-183, 2013.

Hogg, A.G., Hua, Q., Blackwell, P.G., Niu, M., Buck, C.E., Guilderson, T.P., Heaton, T.J., Palmer, J.G., Reimer, P.J., Reimer, R.W., Turney, C.S.M., Zimmerman, S.R.H., SHCal13 Southern Hemisphere Calibration, 0–50,000 Years cal BP, Radiocarbon, 55, 1889-1903, 2016.

Holmgren, K., Karlén, W., Lauritzen, S.E., Lee-Thorp, J.A., Partridge, T.C., Piketh, S., Repinski, P., Stevenson, C., Svanered, O., Tyson, P.D.: A 3000-year high-resolution stalagmite based record of palaeoclimate for northeastern South Africa, Holocene, 9, 295-309, 1999.

Hua, Q., Barbetti, M., Rakowski, A.Z.: Atmospheric Radiocarbon for the Period 1950–2010, Radiocarbon, 55, 2059-2072, 2016.

Hudson, D.A., Hewitson, B.C.: The atmospheric response to a reduction in summer Antarctic sea-ice extent, Clim. Res., 16, 79-99. 2001

Huffman, T.N.: Intensive El Niño and the Iron Age of South-eastern Africa. J. Archaeol. Sci., 37, 2572-2586, 2010.

Humphries, M.S., Benitez-Nelson, C.R., Bizimis, M., Finch, J.M.: An aeolian sediment reconstruction of regional wind intensity and links to larger scale climate variability since the last deglaciation from the east coast of southern Africa. Global Planet. Change, 156, 59-67, 2017.

Humphries, M.S., Green, A.N., Finch, J.M.: Evidence of El Niño driven desiccation cycles in a shallow estuarine lake: The evolution and fate of Africa's largest estuarine system, Lake St Lucia. Global Planet. Change, 147, 97-105, 2016.

IAEA/WMO, Global Network of Isotopes in Precipitation, The GNIP Database, http://www.iaea.org/water, last access: June 2018.

Kahmen, A., Schefuß, E., Sachse, D.: Leaf water deuterium enrichment shapes leaf wax n-alkane δD values of angiosperm plants I: Experimental evidence and mechanistic insights, Geochim. et Cosmochim. Ac., 111, 39-49, 2013.

Kim, K., Lee, X.: Isotopic enrichment of liquid water during evaporation from water surfaces. J. Hydrol., 399, 364-375, 2011.

Kruger, A.C., Goliger, A.M., Retief, J.V., Sekele, S.: Strong wind climatic zones in South Africa. Wind Struct., 13, 37-55, 2010.

Lamy, F., Hebbeln, D., Röhl, U., Wefer, G., Holocene rainfall variability in southern Chile: a marine record of latitudinal shifts of the Southern Westerlies, Earth Planet. Sci. Lett., 185, 369-382, 2001.

Lamy, F., Kilian, R., Arz, H.W., Francois, J.-P., Kaiser, J., Prange, M., Steinke, T.: Holocene changes in the position and intensity of the southern westerly wind belt, Nat. Geosci., 3, 695-699. 2010.

Laskar, J., Fienga, A., Gastineau, M., Manche, H.: La2010: a new orbital solution for the long-term motion, Astron. Astrophys., 532, 2011.

Lindesay, J.A.: South African rainfall, the Southern Oscillation and a Southern Hemisphere semi-annual cycle, J. Climatol., 8, 17-30, 1988.

Mason, S.J., Jury, M.R., Climatic variability and change over southern Africa: a reflection on underlying processes, Prog. Phys. Geog., 21, 23-50. 1997.

Meadows, M.E., Baxter, A.J.: Holocene vegetation history and palaeoenvironments at Klaarfontein Springs, Western Cape, South Africa, Holocene, 11, 699-706, 2001.

Mejía, L.M., Ziveri, P., Cagnetti, M., Bolton, C., Zahn, R., Marino, G., Martínez-Méndez, G., Stoll, H.: Effects of midlatitude westerlies on the paleoproductivity at the Agulhas Bank slope during the penultimate glacial cycle: Evidence from coccolith Sr/Ca ratios, Paleoceanography, 29, 697-714, 2014.

Moy, C.M., Seltzer, G.O., Rodbell, D.T., Anderson, D.M.: Variability of El Nino/Southern Oscillation activity at millenial timescales during the Holocene epoch, Nature, 420, 162-165, 2002.

Neumann, F.H., Scott, L., Bousman, C.B., van As, L., A Holocene sequence of vegetation change at Lake Eteza, coastal KwaZulu-Natal, South Africa, Rev. Palaeobot. Palyno., 162, 39-53, 2010.

Nicholson, S.E., Flohn, H.: African environmental and climatic changes and the general atmospheric circulation in late pleistocene and holocene, Climatic Change, 2, 313-348, 1980.

Otto-Bliesner, B.L., Brady, E.C., Clauzet, G., Tomas, R., Levis, S., Kothavala, Z., Last Glacial Maximum and Holocene Climate in CCSM3, J. Clim., 19, 2526-2544, 2006.

Clim. Past Discuss., https://doi.org/10.5194/cp-2019-4
Manuscript under review for journal Clim. Past
Discussion started: 21 January 2019

Partridge, T.C., Demenocal, P.B., Lorentz, S.A., Paiker, M.J., Vogel, J.C.: Orbital forcing of climate over South Africa: A 200,000-year rainfall record from the pretoria saltpan, Quaternary Sci.Rev., 16, 1125-1133, 1997.

Reason, C.J.C., Mulenga, H.: Relationships between South African rainfall and SST anomalies in the Southwest Indian Ocean, Int. J. Climatol., 19, 1651-1673, 1999.

Rodbell, D.T., Seltzer, G.O., Anderson, D.M., Abbott, M.B., Enfield, D.B., Newman, J.H.: A ~15,000-Year Record of El Niño-Driven Alluviation in Southwestern Ecuador, Sci. J., 283, 516-520, 1999.

Rojas, M., Moreno, P., Kageyama, M., Crucifix, M., Hewitt, C., Abe-Ouchi, A., Ohgaito, R., Brady, E.C., Hope, P.: The Southern Westerlies during the last glacial maximum in PMIP2 simulations. Clim. Dynam., 32, 525-548, 2009.

Sachse, D., Billault, I., Bowen, G.J., Chikaraishi, Y., Dawson, T.E., Feakins, S.J., Freeman, K.H., Magill, C.R., McInerney, F.A., van der Meer, M.T.J., Polissar, P., Robins, R.J., Sachs, J.P., Schmidt, H.-L., Sessions, A.L., White, J.W.C., West, J.B., Kahmen, A.: Molecular Paleohydrology: Interpreting the Hydrogen-Isotopic Composition of Lipid Biomarkers from Photosynthesizing Organisms. Annu. Rev. Earth Pl. Sc., 40, 221-249, 2012.

Sandweiss, D.H., Richardson, J.B., Reitz, E.J., Rollins, H.B., Maasch, K.A.: Geoarchaeological Evidence from Peru for a 5000 Years B.P, Onset of El Niño. Sci. J., 273, 1531-1533, 1996.

Schmidt, F., Oberhänsli, H., Wilkes, H.: Biocoenosis response to hydrological variability in Southern Africa during the last 84kaBP: A study of lipid biomarkers and compound-specific stable carbon and hydrogen isotopes from the hypersaline Lake Tswaing, Global Planet. Change, 112, 92-104, 2014.

Schefuß, E., Kuhlmann, H., Mollenhauer, G., Prange, M., Pätzold, J., Forcing of wet phases in southeast Africa over the past 17,000 years, Nature, 480, 509, 2011

Schefuß, E., Schouten, S., Schneider, R.R., Climatic controls on central African hydrology during the past 20,000 years, Nature, 437, 1003-1006, 2005.

Scott, L., Holmgren, K., Talma, A.S., Woodborne, S., Vogel, J.C.: Age interpretation of the Wonderkrater spring sediments and vegetation change in the Savanna Biome, Limpopo province, South Africa : research letter, S. Afr. J. Sci., 99, 484-488, 2003.

Scott, L., Vegetation history and climate in the Savanna biome South Africa since 190,000 ka: a comparison of pollen data from the Tswaing Crater (the Pretoria Saltpan) and Wonderkrater. Quatern. Int., 57-58, 215-223, 1999.

Scott, L.: Fluctuations of vegetation and climate over the last 75 000 years in the Savanna Biome, South Africa: Tswaing Crater and Wonderkrater pollen sequences reviewed, Quaternary Sci. Rev., 145, 117-133, 2016.

Scott, L., Neumann, F.H., Brook, G.A., Bousman, C.B., Norström, E., Metwally, A.A.: Terrestrial fossil-pollen evidence of climate change during the last 26 thousand years in Southern Africa, Quaternary Sci. Rev., 32, 100-118, 2012.

Simon, M.H., Ziegler, M., Bosmans, J., Barker, S., Reason, C.J.C., Hall, I.R.: Eastern South African hydroclimate over the past 270,000 years, Nature, 5, 18153, 2015.

Sprenger, M., Tetzlaff, D., Soulsby, C.: Soil water stable isotopes reveal evaporation dynamics at the soil–plant–atmosphere interface of the critical zone, Hydrol. Earth Syst. Sci., 21, 3839-3858, 2017.

Stock, W.D., Chuba, D.K., Verboom, G.A.: Distribution of South African C3 and C4 species of Cyperaceae in relation to climate and phylogeny, Austral Ecol., 29, 313-319,2004.

Stone, A.E.C., Last Glacial Maximum conditions in southern Africa, Prog. Phys.l Geog., 38, 519-542, 2014.

Stuut, J.-B.W., Lamy, F.: Climate variability at the southern boundaries of the Namib (southwestern Africa) and Atacama (northern Chile) coastal deserts during the last 120,000 yr, Quaternary Res., 62, 301-309, 2004.

Taylor, R., Kelbe, B., Haldorsen, S., Botha, G.A., Wejden, B., Været, L., Simonsen, M.B.: Groundwater-dependent ecology of the shoreline of the subtropical Lake St Lucia estuary, Environ. Geol., 49, 586-600, 2006.

Clim. Past Discuss., https://doi.org/10.5194/cp-2019-4
Manuscript under review for journal Clim. Past
Discussion started: 21 January 2019

Tierney, J.E., Russell, J.M., Huang, Y., Sinninghe Damste, J.S., Hopmans, E.C., Cohen, A.S.: Northern hemisphere controls on tropical southeast African climate during the past 60,000 years, Sci. J., 322, 252-255, 2008.

Tipple, B.J., Meyers, S.R., Pagani, M.: Carbon isotope ratio of Cenozoic CO2: A comparative evaluation of available geochemical proxies, Paleoceanography, 25, 1-11, 2010.

Toggweiler, J.R., Russell, J.L., Carson, S.R.: Midlatitude westerlies, atmospheric CO2, and climate change during the ice ages, Paleoceanography, 21, 1-15, 2006.

Tudhope, A.W., Chilcott, C.P., McCulloch, M.T., Cook, E.R., Chappell, J., Ellam, R.M., Lea, D.W., Lough, J.M., Shimmield, G.B.: Variability in the El Niño-Southern Oscillation Through a Glacial-Interglacial Cycle, Sci. J., 291, 1511-1517, 2001.

Tyson, P.D.: Atmospheric circulation changes and palaeoclimates of southern Africa, S. Afr. J. Sci., 95, 194-201, 1999.

Tyson, P.D.: Climatic Change and Variability in Southern Africa, Oxford University Press, Cape Town, 1986.

Venter, C.E.: The Vegetation Ecology of Mfabeni Peat Swamp, St Lucia, KwaZulu-Natal, University of Pretoria, Pretoria, 2003.

Vogts, A., Badewien, T., Rullkötter, J., Schefuß, E.: Near-constant apparent hydrogen isotope fractionation between leaf wax n-alkanes and precipitation in tropical regions: Evidence from a marine sediment transect off SW Africa, Org. Geochem., 96, 18-27, 2016.

Vogel, J.C., Fuls, A., Ellis, R.P.: The geographical distribution of kranz grasses in south africa, S. Afr. J. Sci., 74, 209-215, 1978.

Waelbroeck, C., Labeyrie, L., Michel, E., Duplessy, J.C., McManus, J.F., Lambeck, K., Balbon, E., Labracherie, M.: Sea-level and deep water temperature changes derived from benthic foraminifera isotopic records, Quaternary Sci. Rev., 21, 295-305, 2002.

Walker, N.D.: Links between South African summer rainfall and temperature variability of the Agulhas and Benguela Current systems, J. Geophys. Res-Occeans, 95, 3297-3319, 1990.

Wang, Y.V., Leduc, G., Regenberg, M., Andersen, N., Larsen, T., Blanz, T., Schneider, R.R.: Northern and southern hemisphere controls on seasonal sea surface temperatures in the Indian Ocean during the last deglaciation, Paleoceanography, 28, 619-632, 2013.

West, A.G., February, E. C., Bowen, G.J.: Spatial analysis of hydrogen and oxygen stable isotopes ("isoscapes") in ground water and tap water across South Africa, J. Geochem. Explor., 145, 213-222, 2014.

Williams, G.P., Bryan, K.: Ice Age Winds: An Aquaplanet Model, J. Climate ,19, 1706-1715, 2006.

Williamson, G.: Preliminary account of the Floristic Zones of the Sperrgebiet (Protected Diamond Area) in southwest Namibia, Dinteria, 1-68, 1997.

World Weather Online: https://www.worldweatheronline.com/saint-lucia-estuary-weather-averages/kwazulu-natal/za.aspx, last access: 9 May 2018.

Wündsch, M., Haberzettl, T., Cawthra, H.C., Kirsten, K.L., Quick, L.J., Zabel, M., Frenzel, P., Hahn, A., Baade, J., Daut, G., Kasper, T., Meadows, M.E., Mäusbacher, R.: Holocene environmental change along the southern Cape coast of South Africa – Insights from the Eilandvlei sediment record spanning the last 8.9 kyr, Global Planet. Change, 163, 51-66, 2018.

Zhao, X., Dupont, L., Schefuß, E., Meadows, M.E., Hahn, A., Wefer, G.: Holocene vegetation and climate variability in the winter and summer rainfall zones of South Africa, Holocene, 26, 843-857, 2016.

Clim. Past Discuss., https://doi.org/10.5194/cp-2019-4
Manuscript under review for journal Clim. Past
Discussion started: 21 January 2019

Climate of the Past
Discussions
Open Access

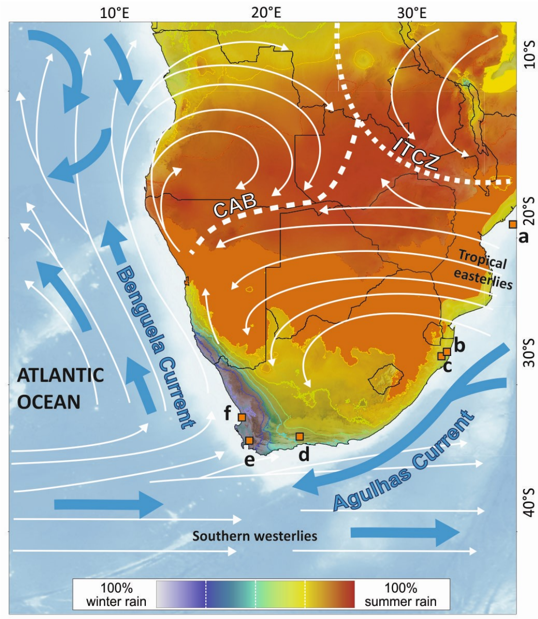

Figure 1.

Climate of the Past Discussions
Open Access
EGU

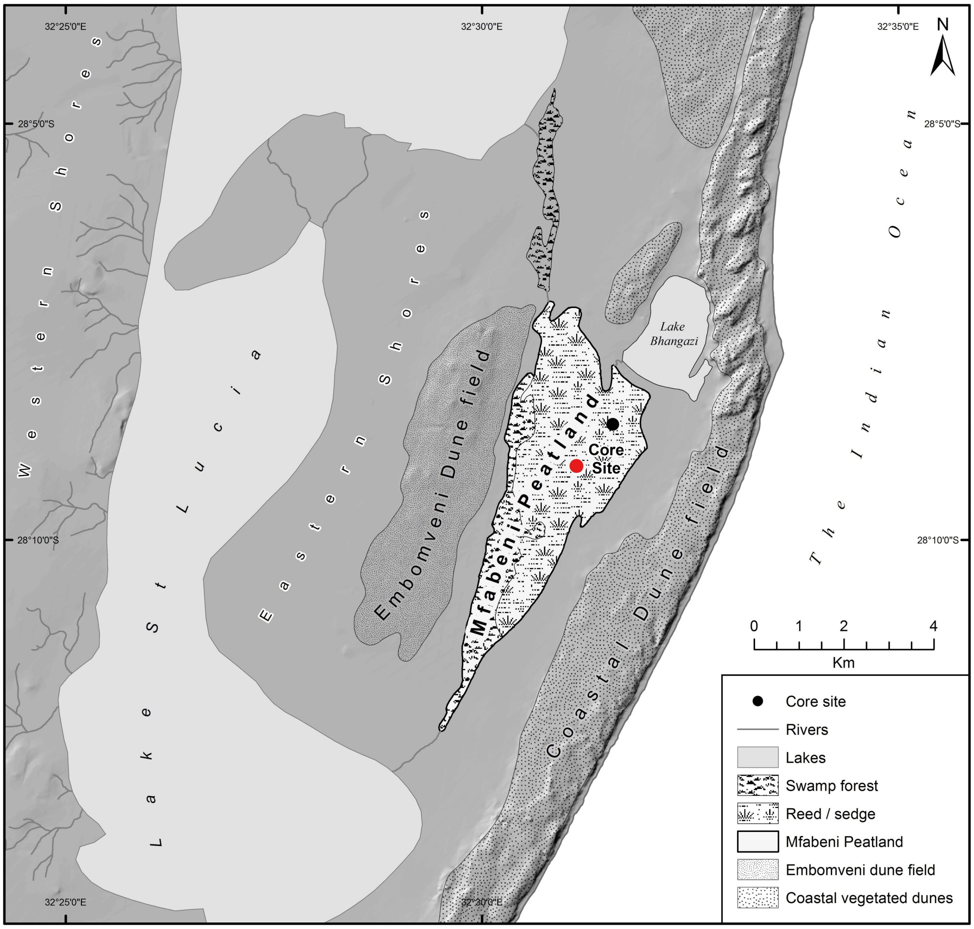

Figure 2.

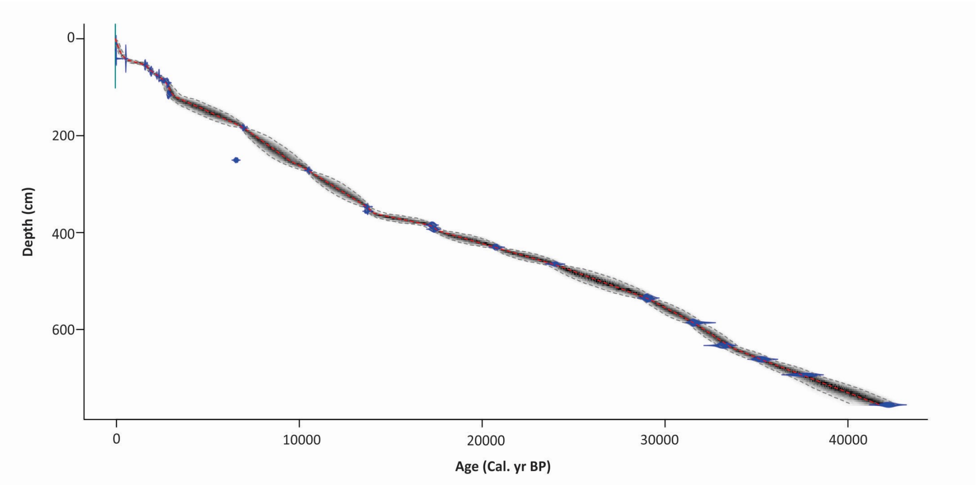

Figure 3.

Climate of the Past Discussions
Open Access

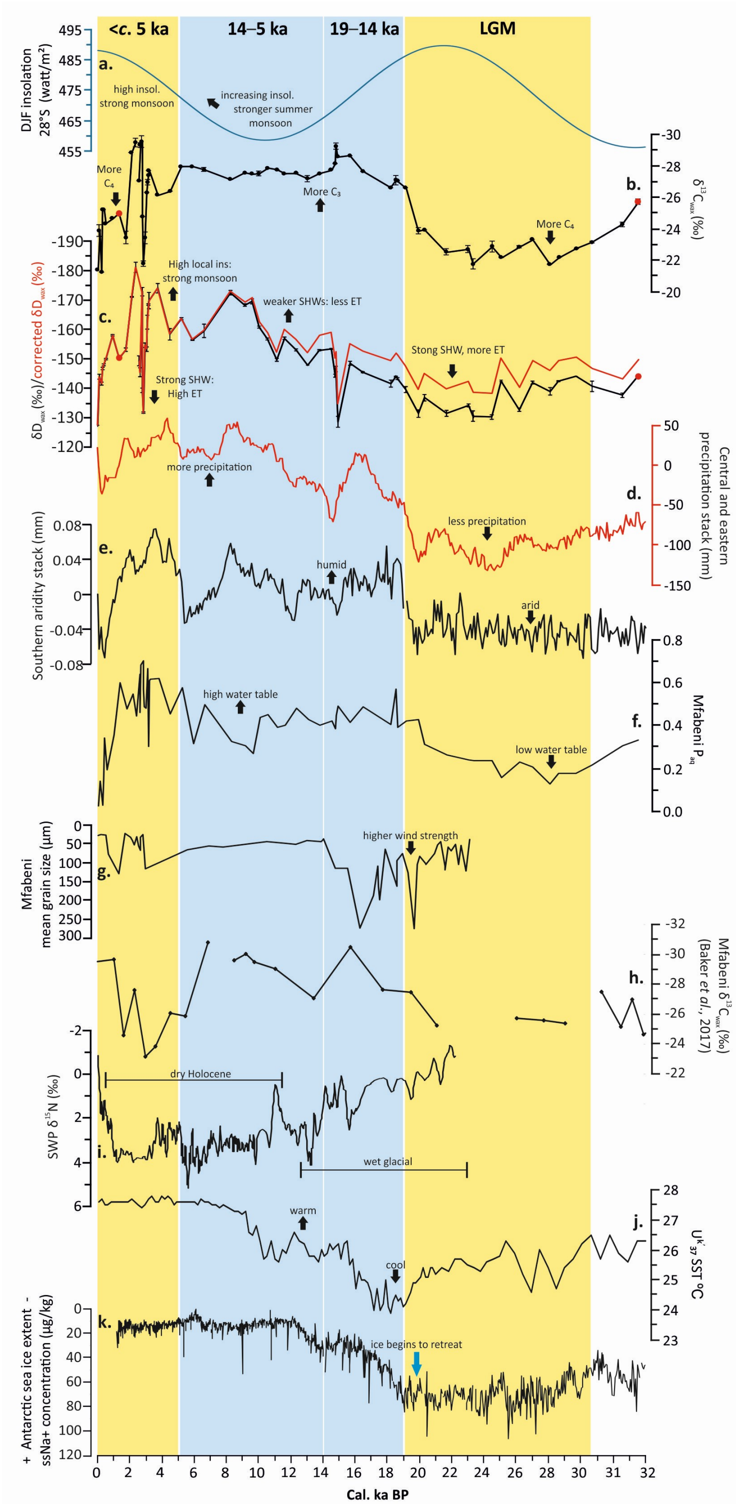

Figure 4.

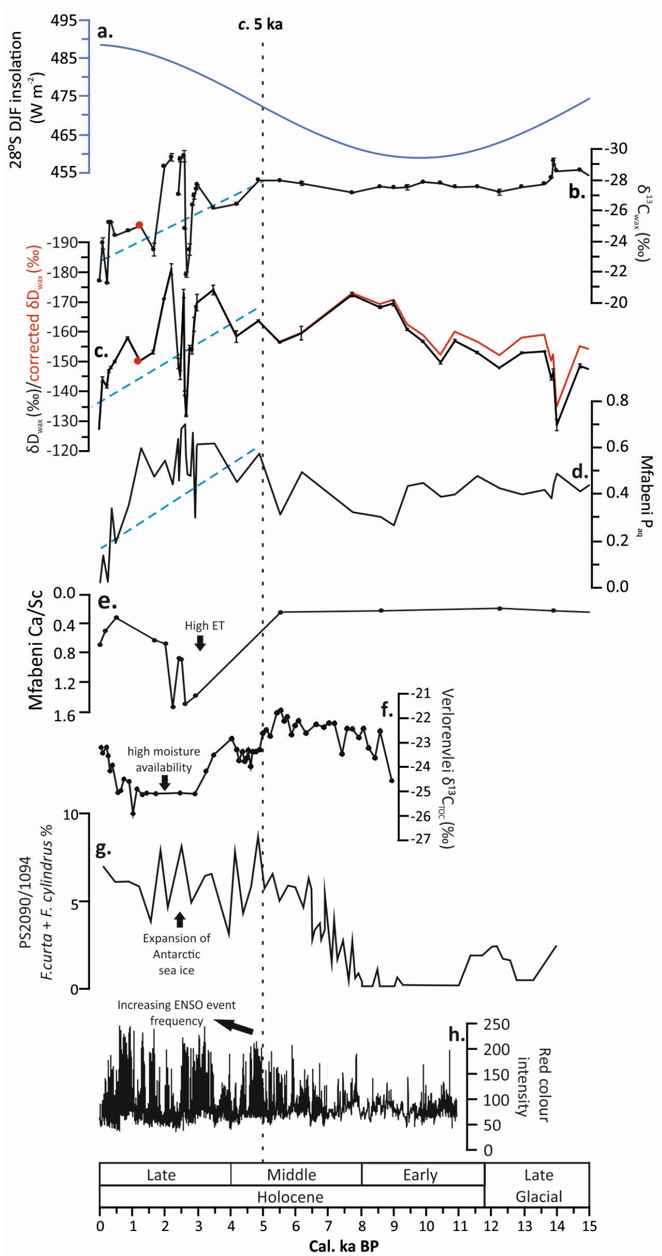
c. 5 ka
a.
28°S DJF insolation (W m-2)
495
485
475
465
455
b.
δ13Cwax (‰)
-30
-28
-26
-24
-22
-20
c.
δDwax (‰)/corrected δDwax (‰)
-190
-180
-170
-160
-150
-140
-130
-120
d.
Mfabeni Paq
0.8
0.6
0.4
0.2
0.0
e.
Mfabeni Ca/Sc
0.0
0.4
0.8
1.2
1.6
High ET
f.
Verlorenvlei δ13CTOC (‰)
-21
-22
-23
-24
-25
-26
-27
high moisture availability
g.
PS2090/1094 F.curta + F. cylindrus %
10
5
0
Expansion of Antarctic sea ice
Increasing ENSO event frequency
h.
Red colour intensity
250
200
150
100
50
0
Late
Middle
Early
Holocene
Late Glacial
0 1 2 3 4 5 6 7 8 9 10 11 12 13 14 15
Cal. ka BP

Figure 5.

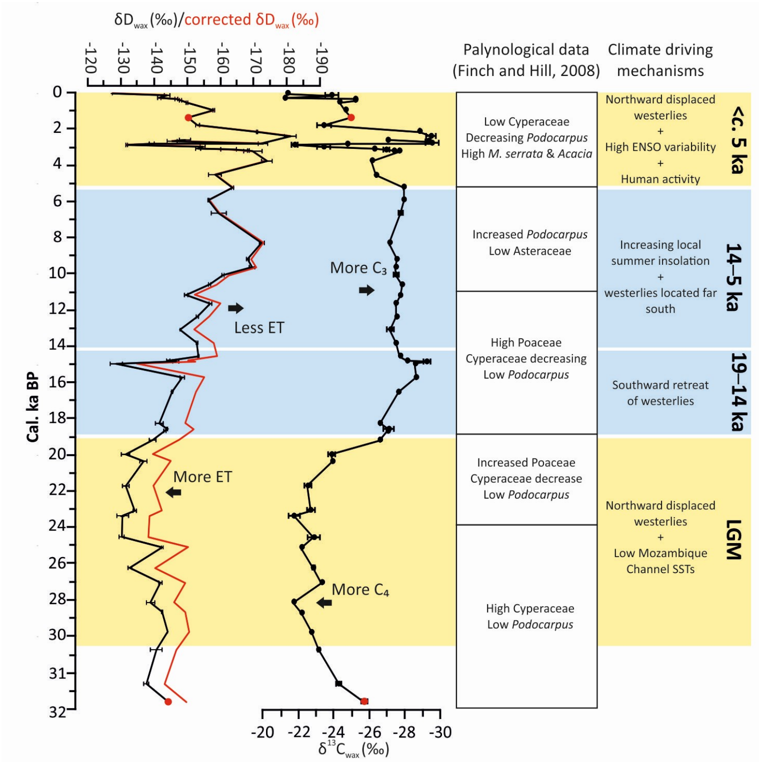
δDwax (‰)/corrected δDwax (‰)
Palynological data (Finch and Hill, 2008)
Climate driving mechanisms
Cal. ka BP
Low Cyperaceae
Decreasing Podocarpus
High M. serrata & Acacia
Northward displaced westerlies
+
High ENSO variability
+
Human activity
<c. 5 ka
Increased Podocarpus
Low Asteraceae
Increasing local summer insolation
+
westerlies located far south
14–5 ka
More C3
Less ET
High Poaceae
Cyperaceae decreasing
Low Podocarpus
Southward retreat of westerlies
19–14 ka
Increased Poaceae
Cyperaceae decrease
Low Podocarpus
More ET
Northward displaced westerlies
+
Low Mozambique Channel SSTs
LGM
High Cyperaceae
Low Podocarpus
More C4
δ13Cwax (‰)

Figure 6.